J. Fluid Mech. (1982), *vol.* 117, *pp.* 507–530
Printed in Great Britain

Two-dimensional inflated buildings in a cross wind

By B. G. NEWMAN AND D. GOLAND
Department of Mechanical Engineering, McGill University, Montreal, Quebec

(Received 18 July 1980 and in revised form 18 August 1981)

Model experiments have been done on two-dimensional inflated buildings in thick boundary layers that simulate either an onshore wind, or flow over sparsely wooded country. A theory has been developed which replaces the boundary layer by an inviscid flow of uniform vorticity. The replacement flow matches both the velocity and the velocity gradient of the wind at the maximum height of the building. The tension in the membrane is quite well predicted by the theory, but the external pressure is in general too low owing to the presence of separation bubbles at the leading and trailing edges.

1. Introduction

The design of inflated buildings must take account of the anticipated loads due to the weather, in particular the loads due to ice, snow and wind. Wind loading is the particular concern of the present paper.

A study has been made of wind flow over a two-dimensional inflated building when the wind is blowing at right angles to the axis of the building. Inflated buildings were first proposed for field hospitals by Lanchester in 1917 and were the subject of a patent at that time. Subsequent applications have been described by Otto & Trostel (1973). Spherical inflated radomes were developed by Bird & Kamrass (1956). Wind-tunnel model tests were made to determine pressure distributions, membrane stresses and to detect any instabilities at low inflation pressures (Kamrass 1954). Later models of inflated hemispheres and cylindrical buildings with quarter-spherical ends were tested by Beger & Macher (1967) and by Niemann (1972). Such shapes have been used as full-scale buildings to cover shopping centres and sports facilities, and as storage buildings and greenhouses (Herzog 1976).

The wind-tunnel model tests referred to above provided necessary design information for specific shapes of building; however, they did not give more general design rules or support development of a general theory for membrane stresses and the external pressure distribution. In addition the Earth's boundary layer was not correctly simulated.

A theory has been developed recently by Newman & Tse (1980), but for a simpler situation. Uniform flow over a thin inflated symmetrical lenticular aerofoil was considered. This type of aerofoil is a reflection-plane model for a two-dimensional inflated building when boundary-layer effects are neglected. In the present paper a theory is developed for boundary-layer flow at right angles to a quasi-two-dimensional building for various heights h of building and for various internal pressures P. With the width or chord of the building denoted by c, tests have been made for wind-off values of h/c ranging from 0·19 to 0·33. The internal pressure is expressed non-dimensionally as

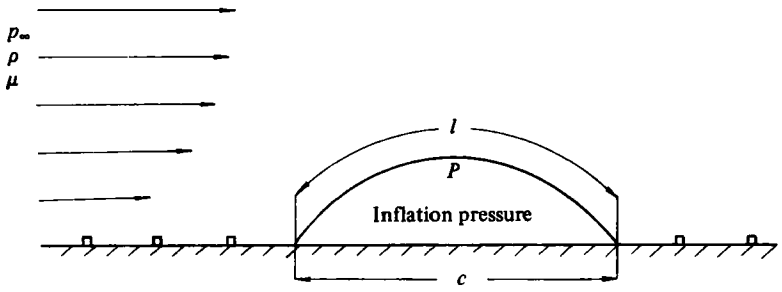

FIGURE 1. Wind flow at right angles to a two-dimensional inflated building.

a coefficient $C_{P_\tau} = (P-p_\infty)/\frac{1}{2}\tau_w$, where p_∞ is the upstream static pressure and τ_w is the boundary-layer skin friction at the location of the model, but in the absence of the model. The values of C_{P_τ} for the tests ranged from 0 to 1400. The Reynolds number $c(\tau_w/\rho)^{\frac{1}{2}}/\nu$ was between 4000 and 6000. The tests were made in two very thick boundary layers representative in the first case of an onshore wind, and in the second case of wind flow over sparsely wooded country. Measurements included membrane tension, membrane angles at the leading and trailing edges, pressure distributions, flow separation and reattachment, and a visual assessment of membrane stability.

A theoretical solution was obtained by replacing the boundary-layer velocity profile by an ideal flow of uniform vorticity with a slip velocity at the boundary. For such a situation it is permissible to superimpose surface sources and sinks to represent the building. The original method was given by Hess & Smith (1967) for rigid bodies. For flexible bodies the final shape of the building was obtained iteratively, assuming, as a first guess, a circular shape and repeatedly calculating the new shape using the relation between the membrane tension, local pressure difference across the membrane, and local radius of curvature of the membrane.

2. Theory

2.1. *Dimensional analysis*

The boundary-layer wind has a mean-velocity profile which is usually represented by a power law of the form (Plate 1971; Davenport 1963)

$$\frac{U}{U_e} = \left(\frac{y}{\delta}\right)^{1/n}, \tag{1}$$

where δ is the thickness of the boundary layer, U_e is the gradient wind, and n^{-1} depends on the roughness of the terrain.

δ is large and of the order of several-hundred metres. The height of the building is usually less than 40 m. Thus the building lies within the wall-law region of the Earth's boundary layer and the aerodynamic forces on the building are established by the skin friction τ_w and the exponent n^{-1}. Hence the criteria of similarity for this situation are

$$\frac{l}{c}, \quad \frac{P-p_\infty}{\frac{1}{2}\rho U_\tau^2}, \quad \frac{1}{n}, \quad \frac{U_\tau c}{\nu}, \quad \frac{w}{P-p_\infty},$$

where w is the membrane weight per unit area and U_τ is the skin-friction velocity $\tau_w^{\frac{1}{2}}\rho^{-\frac{1}{2}}$ (see figure 1).

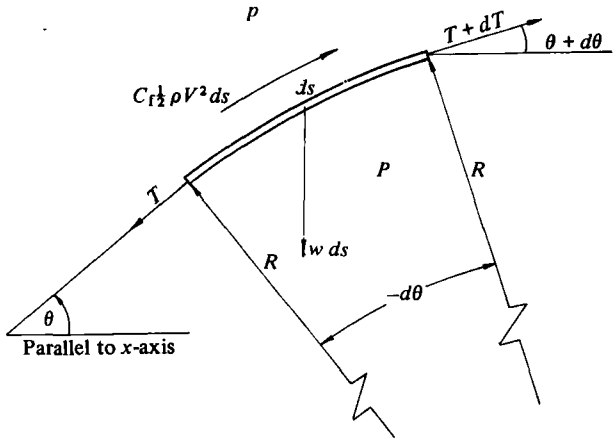

FIGURE 2. Forces acting on a small length ds of membrane.

At high-enough Reynolds numbers it is possible that the dependence on Reynolds number will be small. At high $(P-p_\infty)/\frac{1}{2}\rho U_r^2$ the shape of the building and with it the external-pressure distribution become independent of P. The parameter $w/(P-p_\infty)$ will be unimportant when it is small. The remaining parameters l/c and n^{-1} retain their importance for all values. The non-dimensional dependent parameters that are usually of interest are the local-pressure coefficient $(p-p_\infty)/\frac{1}{2}\rho U_r^2$ and the membrane-tension coefficient $T/\frac{1}{2}\rho U_r^2 c$. Strictly speaking $T/\frac{1}{2}\rho U_r^2 c$ is also a local parameter. However, it may be shown that the variation of tension within the membrane is usually small and negligible.

2.2. *The variation of tension T*

It is usually permissible to assume that the change in tension in the membrane is small enough to be neglected. The changes are due to wind-flow skin friction and membrane weight and these will be considered separately.

The change due to wind friction alone may be stated in terms of the skin friction coefficient C_f (see figure 2).

Resolving parallel to the membrane and ignoring $w\,ds$

$$-dT = C_f \tfrac{1}{2}\rho V^2 ds, \tag{2}$$

where V is the local wind velocity outside the boundary layer that forms on the membrane. Resolving perpendicular to the membrane

$$-T\,d\theta = (P-p)\,ds. \tag{3}$$

Dividing (2) by (3),

$$\frac{dT}{T} = C_f \frac{\frac{1}{2}\rho V^2}{P-p}\,d\theta. \tag{4}$$

If the oncoming flow had a *uniform* velocity U, then

$$\frac{P-p}{\frac{1}{2}\rho V^2} = 1 + (C_P - 1)\left(\frac{U}{V}\right)^2,$$

where

$$C_P = \frac{P-p_\infty}{\frac{1}{2}\rho U^2}.$$

In practice C_P is close to unity; thus $(P-p)/\frac{1}{2}\rho V^2$ is approximately unity and (4) may be integrated to give the approximate expression

$$\ln \frac{T_1}{T_2} = C_f(\theta_1 - \theta_2). \tag{5}$$

For buildings the change of θ from trailing to leading edge is usually less than π and a suitable choice for C_f is 0·003. Thus

$$\frac{T_{te}}{T_{le}} < e^{-0\cdot0094} = 0\cdot99.$$

The change of tension due to wind is therefore negligible.

The change of tension due to membrane weight is considered in the absence of wind skin friction and the force $C_f \frac{1}{2}\rho V^2 ds$ is ignored in figure 2.

Resolving parallel to the membrane,

$$dT = w\,ds \sin\theta, \tag{6}$$

and, resolving perpendicular to the membrane,

$$-T\,d\theta + w\,ds\cos\theta = (P-p)\,ds. \tag{7}$$

Eliminating ds from (6) and (7),

$$-\frac{dT}{T} = \frac{w\sin\theta}{P-p-w\cos\theta}\,d\theta.$$

p varies with s owing to the wind flow, and an average value $\bar{p}$ is adopted in order to integrate this equation. Thus

$$-\ln T = \ln(P-\bar{p}-w\cos\theta) + \text{const.}$$

If T_2 is the tension at the leading edge where $\theta = \theta_2$, and T_0 is the tension at the top of the building where $\theta = 0$, then

$$\frac{T_0}{T_2} = \frac{(P-\bar{p})-w\cos\theta_2}{(P-\bar{p})-w}. \tag{8}$$

Typical values of $w/(P-\bar{p})$ are 0·05 or less for a model building, and also 0·05 or less for a full-scale building that is made of heavier material but operated at higher inflation pressures. The maximum value of $\theta = 90°$ and the maximum value of T_0/T_1 is therefore 1·05. The change of tension due to membrane weight is therefore usually small.

2.3. *Idealization of the boundary-layer velocity profile*

In order to predict the pressure distribution and the shape of the building, two-dimensional ideal-fluid theory is used. The building is represented by an array of distributed sources and sinks placed on the surface of the membrane, as in the method developed by Hess & Smith (1967). Sources and sinks may be superimposed on a rotational flow only for certain cases. One possibility is that the oncoming flow has a uniform vorticity C. If ψ_1 is the stream function for the oncoming flow, then

$$\nabla^2\psi_1 = C;$$

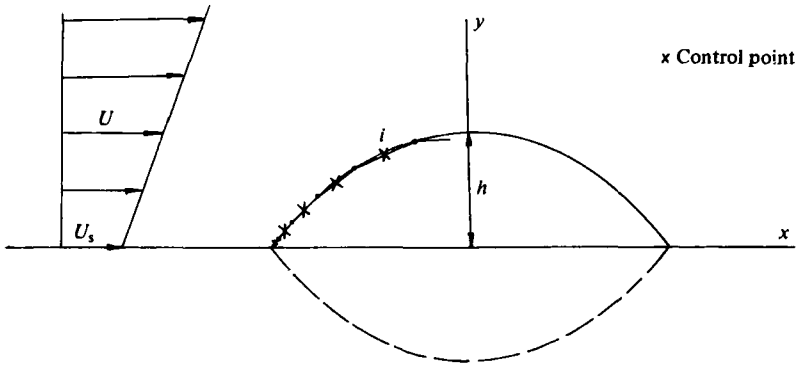

FIGURE 3. Ideal flow of uniform vorticity past an inflated body approximated by straight elements.

and, if ψ_2 is the stream function for the added flow due to the sources and sinks, then

$$\nabla^2\psi_2 = 0.$$

Superposition, represented by $\nabla^2(\psi_1+\psi_2) = C$, is permissible since it satisfies the requirement that the vorticity along an individual streamline remain constant.

The best procedure for matching a flow of uniform vorticity to a boundary-layer flow is not obvious. The inviscid flow is given by (figure 3)

$$\frac{U}{U_s} = 1+\frac{y}{a}, \tag{9}$$

where U_s is the assumed slip velocity at the ground and U_s/a is the vorticity. Both U_s and a are constants.

If the velocity at the top of the building, $y = h$, is made the same as that in the boundary layer, then

$$\frac{U_r}{U_s}\left(\frac{h}{y_r}\right)^{1/n} = 1+\frac{h}{a},$$

where U_r is the wind velocity at some reference height y_r. The gradient wind U_e and the boundary-layer thickness δ are usually used for these reference values in the full-scale situation, but the equivalent values may not exist in a boundary-layer simulation.

One other condition is required to determine U_s and a. Three possibilities were considered:

(i) make the average dynamic pressure from $y = 0$ to $y = h$ the same for both profiles;

(ii) make the slopes of the velocity profiles the same at $y = h$;

(iii) make the slope of the velocity profiles the same at the height corresponding to the average velocity over the height h of the boundary-layer profile.

2.4. *Two-dimensional rotational flow of an ideal fluid past an inflated body*

To preserve the ground as a streamline the flow and the body are reflected in the ground as indicated. Following Hess & Smith (1967), the body, whose shape is assumed in the first instance, is replaced by a many-sided polygon (figure 3).

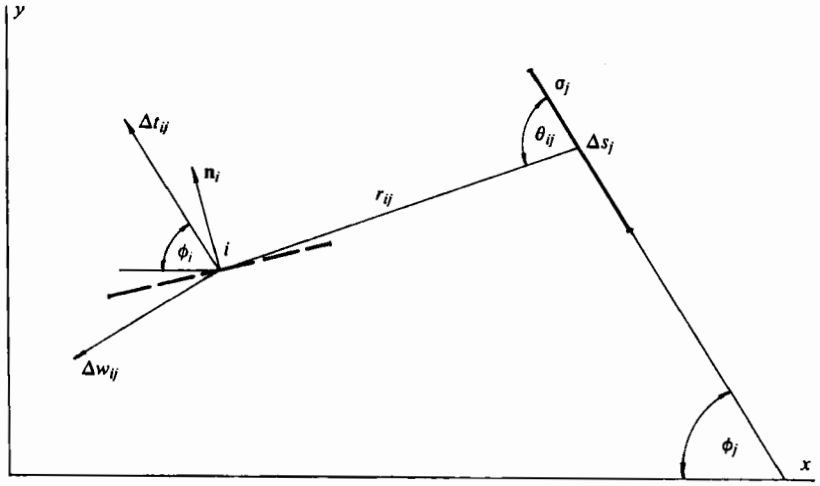

FIGURE 4. Influence of element j on control point i.

Each straight-line element of the polygon is assumed to have a uniform source distribution σ per unit length. The midpoints of the line elements are chosen as control points for expressing the condition that there is no flow perpendicular to the surface. The polygon is chosen so that the line elements are shorter near the leading-edge and trailing-edge stagnation points, while the ratio of the sizes of adjacent elements is made less than 1·5.

The velocity perpendicular to the ith line element due to the local source is $\frac{1}{2}\sigma_i$ out from the body. That due to the source on line element j is $A_{ij}\sigma_j$, where A_{ij} is the influence coefficient for velocity perpendicular to element i.

If $\mathbf{n}_i$ is the outward unit vector perpendicular to i, the local boundary condition becomes

$$\tfrac{1}{2}\sigma_i + \sum_{j=1, j\neq i}^{N} A_{ij}\sigma_j + \mathbf{n}_i . \mathbf{U}_i = 0, \tag{10}$$

where $\mathbf{U}_i$ is the velocity of the oncoming flow at control point i in the absence of the body, and there are N line elements and N control points. $A_{ij}\sigma_j$ is calculated as follows (see figure 4).

The velocity at i, due to a source $\sigma_j\,\Delta s_j$ on the line element Δs_j at j, is obtained by adding up the contributions from each small part of Δs_j (Hess & Smith 1967). The component parallel to Δs_j is

$$\Delta t_{ij} = \frac{\sigma_j}{4\pi} \ln \frac{r_{ij}^2 + r_{ij}\Delta s_j \cos\theta_{ij} + \frac{1}{4}\Delta s_j^2}{r_{ij}^2 - r_{ij}\Delta s_j \cos\theta_{ij} + \frac{1}{4}\Delta s_j^2}, \tag{11}$$

and the component perpendicular to Δs_j is

$$\Delta w_{ij} = \frac{\sigma_j}{2\pi} \arctan \frac{\Delta s_j r_{ij} \sin\theta_{ij}}{r_{ij}^2 - \frac{1}{4}\Delta s^2}. \tag{12}$$

Thus if the unit normal for element i, which is $\mathbf{n}_i$, has components n_{ti} and n_{wi} respectively parallel and perpendicular to Δs_j, then

$$A_{ij}\sigma_j = \Delta t_{ij} n_{ti} - \Delta w_{ij} n_{wi}. \tag{13}$$

As the relative positions and orientations of the elements change, the signs in this expression may change, and procedures are adopted in the numerical analysis to take care of this.

The local speed V_i at the control points is given by

$$V_i^2 = \left\{U_i - \sum_{j=1}^{j=N} (\Delta t_{ij} \cos\phi_j + \Delta w_{ij} \sin\phi_j)\right\}^2 + \left\{\sum_{j=1}^{j=N} (\Delta t_{ij} \sin\phi_j - \Delta w_{ij} \cos\phi_j)\right\}^2, \quad (14)$$

where the angle ϕ_j is shown in figure 4. The associated local-pressure coefficient expressed in terms of U_s is given by

$$(C_p)_i = 1 - \left(\frac{V_i}{U_s}\right)^2. \quad (15)$$

The N unknowns in (10) are σ_i ($i = 1, \ldots, N$). There are N equations, and all are linear in these σ_i. Thus the equations are readily solved by matrix inversion. To reduce the computing time use is made of the double symmetry of the body, the symmetry in the ground and the symmetry about the vertical through the mid-chord. The pressure distribution may therefore be obtained for any chosen shape of the membrane. Initially a circular arc shape was assumed for a given internal pressure $P - p_\infty$, and l/c. Since this shape corresponds to very low wind conditions, the tension T in the membrane is given implicitly by

$$\frac{C_P}{C_T} = \frac{2c}{l} \arcsin \frac{C_P}{2C_T},$$

where

$$C_P = \frac{P - p_\infty}{\frac{1}{2}\rho U^2}, \quad C_T = \frac{T}{\frac{1}{2}\rho U^2 c}.$$

For the particular height of the building, the values of U_s and a are determined by matching the boundary-layer flow. The pressure distribution is calculated in the manner outlined above. The local radius of curvature R is then determined from

$$\frac{R}{c} = \frac{C_T}{C_P - C_p},$$

using the initial value of C_T. Thus a new value of R/c for every x/c is established. If θ is the local slope of the membrane then

$$\frac{c}{R} = \cos\theta \frac{d\theta}{d(x/c)}. \quad (16)$$

The end condition for this equation is that $\theta = 0$ when $x/c = \frac{1}{2}$. Hence θ is known as a function of x/c, and y/c is determined by integrating $d(y/c) = (\tan\theta)\, d(x/c)$.

Thus a new shape y/c as a function of x/c, and a new l/c, is determined. The calculation of the pressure distribution is repeated for the slightly modified values of U_s and a/c corresponding to the new height of the building. Iteration proceeds until the building no longer changes shape to a certain accuracy ((height change)$/c < 10^{-5}$ was chosen). The final iteration establishes the value of l/c corresponding to the assumed values C_P and C_T. It may be noted that these coefficients have so far been normalized using $\frac{1}{2}\rho U_s^2$. However, once the matching procedure is chosen they can readily be converted to values using $\frac{1}{2}\rho U_\tau^2$, and they are then identified by the addition of a suffix τ.

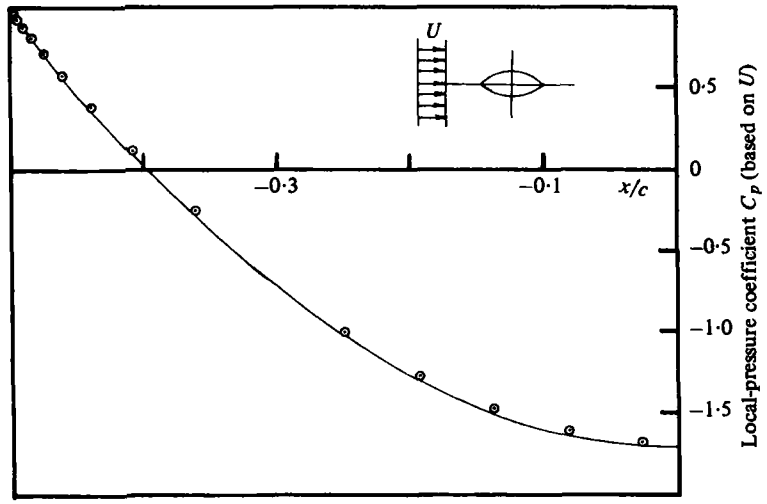

FIGURE 5. Uniform flow past a thin lenticular aerofoil of thickness-to-chord ratio 0·537. ⊙, numerical; ——, exact.

Checks were first run on the method by applying it to uniform flow past rigid bodies. Results were obtained for both a Rankine oval and a circular cylinder, and were compared with the corresponding exact solutions. Good agreement was obtained when 17 elements were used in each quarter of the body. A similar comparison for a lenticular aerofoil of thickness-to-chord ratio of 0·537 is shown in figure 5.

A further comparison was made for the shear flow represented by $U = 1+2|y|$ combined with a doublet of strength 20π, which produced a symmetrical body of chord 2. Using 17 points for each quarter of the body the present method predicted a distribution of pressure that was in excellent agreement with the analytical solution.

2.5. *Solution for small $(l-c)/c$ and c/a of $O(1)$ or less*

For a building of relatively small height, for which $(l-c)/c$ is small, a solution may be obtained without recourse to iteration. The analysis closely follows that of Newman & Tse (1980) for a lenticular aerofoil. The aerofoil shape is now established using sources and sinks *on the aerofoil chord* (the x-axis). The local source strength at point x_1, y_1 is

$$m = 2U_s\left(1+\frac{y_1}{a}\right)\frac{dy_1}{dx_1}. \tag{17}$$

Thus the surface velocity at (x, y) is

$$u = U_s\left(1+\frac{y}{a}\right) - \int_0^c \frac{U_s\left(1+\frac{y_1}{a}\right)\frac{dy_1}{dx_1}dx_1}{\pi(x_1-x)}.$$

Since

$$p_\infty + \tfrac{1}{2}\rho U_s^2 = p + \tfrac{1}{2}\rho u^2 \quad \text{and} \quad P-p = -T\frac{d^2y}{dx^2},$$

then

$$-\tfrac{1}{2}C_T\frac{d^2z}{dx^2} = \frac{1}{2}+\frac{z}{a}-\frac{1}{\pi}\int_0^1 \frac{\left(1+C_P\frac{z_1}{a}\right)\frac{dz_1}{dx_1}dx_1}{x_1-x}, \tag{18}$$

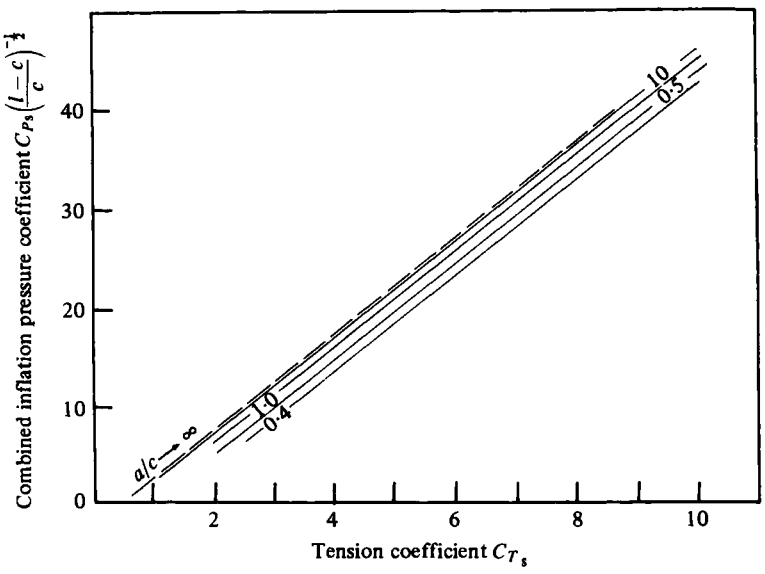

FIGURE 6. Tension coefficient as a function of collapsed pressure coefficient; theoretical results for $h/c < 0{\cdot}10$ and various values of a/c.

where $z = y/cC_P$, $z_1 = y_1/cC_P$, and a and x have been normalized using c. Also

$$\frac{1}{C_P^2}\frac{l-c}{c} = \frac{1}{2}\int_0^1 \left(\frac{dz}{dx}\right)^2 dx. \tag{19}$$

Equation (18) shows that $z(x)$ is determined by C_T and a, if $C_P(z_1/a) = y_1/ac$ is small. Since the maximum value of y_1 is the height of the building, and is thus small compared with c, this requirement becomes that a^{-1} is $O(1)$ or less, which is usually the case in the Earth's boundary layer. It follows that the integral in (19) is also a function of C_T and a. Hence C_T is determined uniquely by $C_P(l-c)^{-\frac{1}{2}}c^{\frac{1}{2}}$ and a/c, where a is now restated as an unnormalized or physical dimension in accordance with (9). This is a generalization of the result for thin lenticular inflated aerofoils in uniform streaming flow for which C_T is a function of $C_P(l-c)^{-\frac{1}{2}}c^{\frac{1}{2}}$ only (Newman & Tse 1980).

In order to check this prediction, the theory of § 2.4 was applied to a range of buildings with $h/c < 0{\cdot}10$, which corresponds to $(l-c)/c$ less than about 0·026. C_T was found to be a unique function of the combined parameter $C_P(l-c)^{-\frac{1}{2}}c^{\frac{1}{2}}$ for each a/c for values of a/c as small as 0·4. The theoretical predictions are shown in figure 6. The result for $a/c \to \infty$ coincides with the result of Newman & Tse (1980). Similar results did not collapse onto one curve for $h/c > 0{\cdot}13$, which corresponds to $(l-c)/c > 0{\cdot}044$.

3. Experiment

3.1. *Apparatus and instruments*

The purpose of the experiments was to test a quasi-two-dimensional model of an inflated building in a relatively thick boundary layer, chosen to simulate the Earth's boundary layer.

The 2 m × 1·5 m blower wind tunnel in the Aerodynamics Laboratory at McGill University was used. In its original form this tunnel had a smaller circular working

section (Vogel 1968). The modified tunnel has a test section 10 m long, so that it is possible to generate a thick boundary layer on the floor. The tunnel is driven by a double-sided centrifugal fan with backward-curved blades and is rated at 30 kW. The maximum tunnel speed in its final configuration was about 7·7 m/s, and tests were made only at this speed. The forces and pressures would have been too difficult to measure at any significantly lower speed or Reynolds number. The long working section of the wind tunnel has an adjustable roof which was set to give constant and thus atmospheric pressure along the working section.

The value of the boundary layer exponent n^{-1} (1) depends on the nature of the terrain and increases with its roughness. For open country $n^{-1} = 0{\cdot}16$ and for sparsely wooded country $n^{-1} = 0{\cdot}24$ (Davenport 1963). These were the chosen values.

The height of full-scale inflated buildings is usually well within the law-of-the-wall region of the Earth's boundary layer, and thus the flow around the buildings is determined by the skin friction and the roughness and is independent of the outer conditions, for example the boundary-layer thickness. Useful model tests may then be made on models which are relatively large as long as they are well within the wall region of the wind-tunnel boundary layer (Cook 1973).

The boundary layer on the floor of the tunnel was artificially thickned using four tapered spires attached to the floor at the entrance to the working section. They were designed according to the procedure described by Campbell & Standen (1969) and Standen (1972) to give a boundary-layer thickness of 1 m and $n^{-1} = 0{\cdot}16$. Roughness was also attached to the floor of the tunnel upstream of the model, over a distance of 9 m. For $n^{-1} = 0{\cdot}16$ a commercial plastic mat with cone-like protrusions was used. The cones were 3 mm high with a 4 mm wide base and were spaced at 28 mm in an hexagonal array. The method of Garshore & de Croos (1977) for rectàngular roughness was used as a guide in choosing this roughness. To simulate a boundary layer with $n^{-1} = 0{\cdot}24$ the same spires were used, but the downstream roughness was increased by replacing the plastic mat with a canvas carpet to which were attached 12 mm × 12 mm strips of wood spaced at 250 mm to form an array of two-dimensional roughness. In both simulations the thickness of the wall region, which limits the height of the models, was approximately 300 mm.

The model buildings were mounted in the centre of the tunnel and had a span of 650 mm and a width, or chord, of 250 mm. The membrane length l was varied from 272·5 mm to 316·5 mm depending on the height of the model building (figure 7). Thin impervious nylon cloth, of mass 25 g/m^2, was used for the membrane. Air from a small blower was supplied through a perforated pipe to the inside of the model at up to 44 Pa gauge. The ends of the model abutted against acrylic plates. An extra 5 mm of cloth was allowed at each end of the membrane, which was tucked under to reduce the leakage of air over these end plates. Two rigid dummy models of about the same height and of circular section were mounted on either side of the acrylic plates so that the model and dummies completely spanned the 2 m width of the tunnel. In this way quasi-two-dimensional conditions over the model could be obtained.

The leading and trailing edges of the membrane were clamped to spanwise cross beams which were each mounted on pairs of flexures. Strain gauges were glued to the flexures to measure the fore and after force on each end of the membrane and ultimately the tension in the membrane. The maximum movement of each beam was less than 1 mm. To seal the region below the model and also prevent air leaking out at the

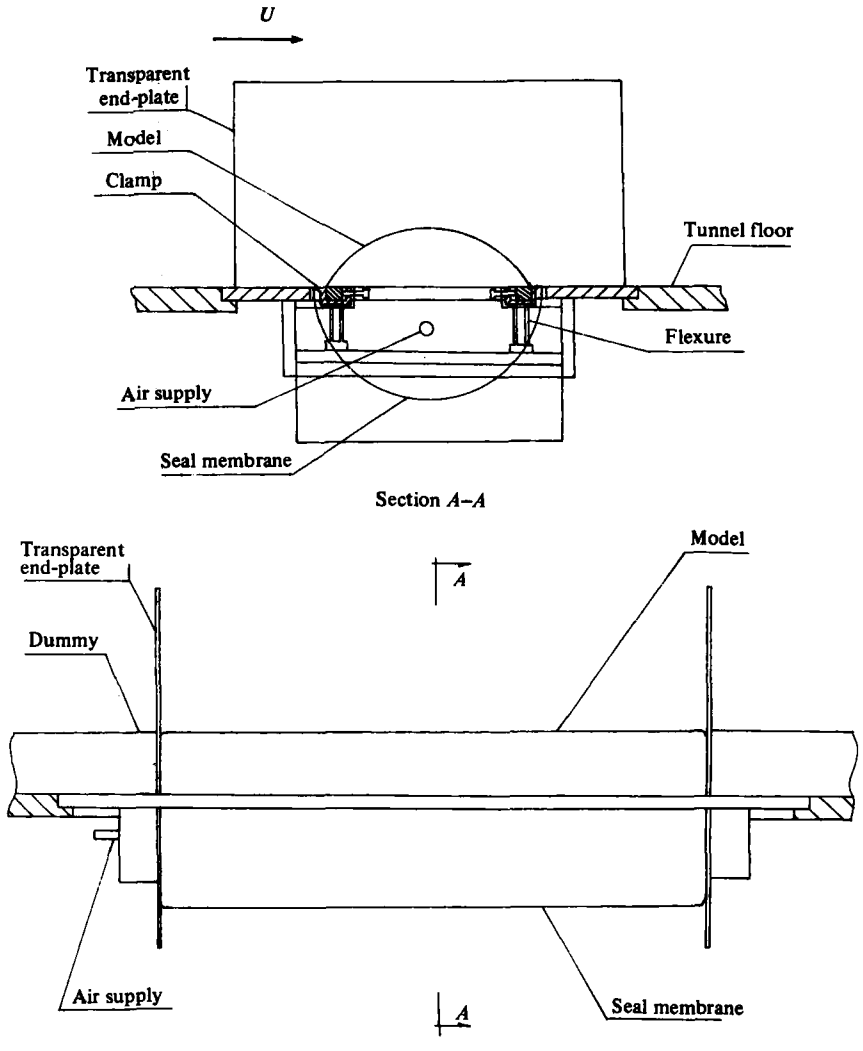

FIGURE 7. Model of a two-dimensional inflated building showing the experimental arrangement.

leading and trailing edges, a second membrane was attached to the cross beams *below* the floor of the tunnel. This seal was designed to be a semicircle so that the tension in it would not affect the forces measured by the strain-gauge system. In practice, small corrections were needed which depended on the actual geometry and on the pressure inside the membrane.

The gauge pressure inside the model was measured with three tubes located at different spanwise positions. Their readings agreed within 1 %. A static tube was used to measure the pressure distribution at the surface of the model. It was held in a traversing gear which enabled it to be placed close to and aligned with the surface locally. The gap between the tube and the surface was less than 0·5 mm. An upstream tunnel reference pressure was used to establish the tunnel dynamic pressure. All pressures were measured on inclined reservoir manometers.

The strain gauges for each flexure system formed a full bridge which was connected to a Brüel and Kjaer type 1526 Strain Indicator. A cathetometer was used to measure the inclination of the membrane at the leading and trailing edges. Owing to the presence of the dummy models it was impossible to view the membranes directly in the axial direction. Thus the cathetometer was directed obliquely from above and the graticule of the instrument was lined up on a chord line drawn on the membrane of the model. The model was then deflated and a protractor was placed at the leading or trailing edge and the inclination corresponding to the alignment of the graticule was readily determined to an accuracy of about 1°.

The floor boundary layer was measured in the absence of the model by means of a comb of 18 Pitot tubes. The comb was connected to a manometer to give the mean-velocity distribution. The turbulence shearing stress $-\rho\overline{uv}$ was determined using a single slanting hot wire (Irwin 1972), which was traversed near the floor. The hot wire was controlled with Disa D equipment and the signal was linearized. Integration times were typically 10 s. Check measurements of $-\rho\overline{uv}$ in fully developed turbulent flow down a pipe indicated an error of 3 % or less.

The regions of separation and reattachment of the boundary layer at the front and over the rear of the models were determined using a tuft made from down which was attached to a thin wand. The accuracy was probably no better than 10 mm. The geometry of the models was measured with a ruler to an accuracy of 0·5 mm.

3.2. *Checks on the apparatus and the reduction of errors*

Corrections for the effect of the seal membrane on the reading of the flexures was obtained theoretically from measurements of the geometry of the seal (which is not a perfect semicircle), combined with measurement of the internal pressure.

As an overall check of the system, wind-off measurements were made for each model. The tension in the model membrane was calculated at each end from the flexure readings (corrected for seal effects) and the leading- and trailing-edge angles, and then compared with the value calculated from the internal pressure and the calculated values of curvature of the membrane. The agreement was good and typically within ± 2 %. It was found that there was no detectable extension of the membrane for the range of pressures which was used (0–44 Pa).

With wind on, the effectiveness of the rigid dummy models on either side of two typical test models was determined by removing them completely. The effect on membrane tension was less than $\frac{1}{2}$ % in both cases. It was therefore concluded that the dummies which were used were more than adequate.

Measurements of the boundary layer behind the spires for the two types of roughness were made at the model position in the absence of the model. The thickness of the boundary layer was about 1·4 m and therefore almost completely filled the tunnel. The velocity profile was plotted logarithmically to determine the value of n^{-1} for the power profile in each case.

Measurements were made at three spanwise positions to check two-dimensionality. Traverses were made at the centre line, which was directly downstream of the mid-point between the two central spires, and at two stations 200 mm on either side, each of which was directly downstream of the spires. For roughness 1, n^{-1} was 0·13 on the centre line, and 0·13 and 0·11 on either side. For roughness 2 the values were 0·24 on the centre line and 0·23 and 0·20 on either side. The centre-line values were adopted

Roughness number	Power n^{-1}	U_τ (m/s) hot wire	U_τ (m/s) law of the wall	U_τ (m/s) velocity-defect law	Maximum tunnel speed (m/s)
1	0·13	0·33	0·24	0·23	7·9
2	0·24	0·37	0·34	0·36	7·5

TABLE 1. Data for experimental mean-velocity profile

for the purpose of comparing theory with experiment. They compare with the design values of 0·16 and 0·24.

The mean-velocity results were replotted in a semi-logarithmic manner to determine the skin friction from the slope of the logarithmic law of the wall,

$$\frac{U}{U_\tau} = \frac{1}{0{\cdot}42} \ln \frac{yU_\tau}{\nu} + f\left(\frac{kU_\tau}{\nu}\right),$$

in the region $y < \frac{1}{4}\delta$. The skin friction was also obtained from the defect law by computing the average velocity U_{av} in the boundary layer and using the formula $(U_e - U_{av})/U_\tau = 3{\cdot}95$ (Coles 1956; Smith & Walker 1958). The values for the two roughnesses are tabulated in table 1, where they are compared with the values obtained from hot-wire readings of $-\rho\overline{uv}$ extrapolated to the surface. It is seen that the agreement is much better for roughness 2 than it is for roughness 1. The disagreement for roughness 1 is attributed to the strong downstream effect of the spires when it is followed by only a slightly rough surface. Apparently the upstream turbulence generated by the spires persists and leads to spuriously high values of $-\rho\overline{uv}$. The values of U_τ that were adopted were those from the mean-velocity measurements because it was considered that the mean velocity is much more significant than the turbulence in establishing the pressure and tension in the membrane. The values are 0·24 m/s for roughness 1 and 0·35 m/s for roughness 2. (See table 1.)

At the suggestion of one of the referees further measurements were made on roughness 2 in order to determine the scale of the turbulence. Following Cook (1977) the mean velocity in the boundary layer was represented by

$$U = \frac{U_\tau}{0{\cdot}41} \ln\left(\frac{z-d}{z_0}\right).$$

Measurements were made at the model position on the smooth surface just downstream of the roughness using a normal linearized hot wire (Disa D equipment). Taking $d = 0$ the values of z_0 were found to be 0·083 mm along the centre line (between spires) and 0·073 mm offset and in the wake of one spire. The fluctuating signal from the anemometer was fed into an H.P. 5420A Digital Signal Analyzer to determine the frequency spectrum of the longitudinal turbulence. This was matched to the standard spectrum given by Cook (1977). As expected the resulting scale factor S varied only slightly with distance from the surface. S varied from 440 to 540 on the centre line and from 470 to 550 at the offset station. Thus the scale factor from the present simulation is about 500, which means that the width of the corresponding full-scale building would be 125 m.

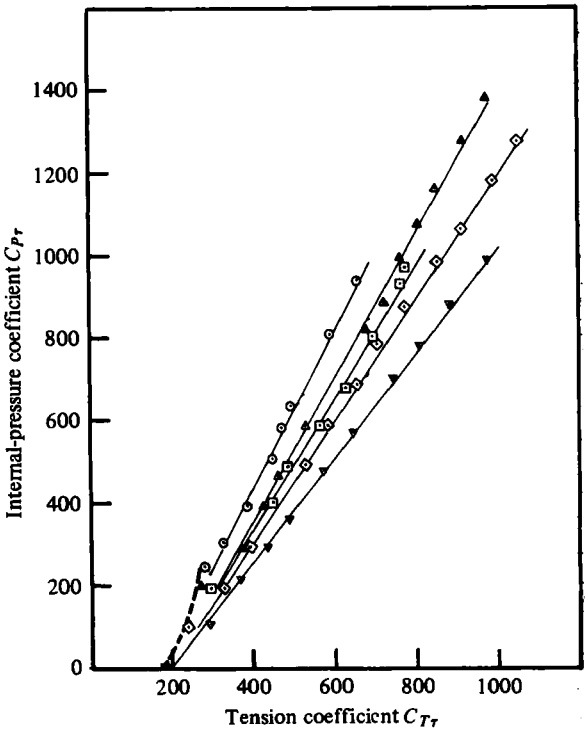

FIGURE 8. Measured tension as a function of inflation pressure for roughness 1. ▽, $(l-c)/c$ = 0·090; ◇, 0·154; ⊡, 0·164; △, 0·231; ⊙, 0·266; – – –, instability line.

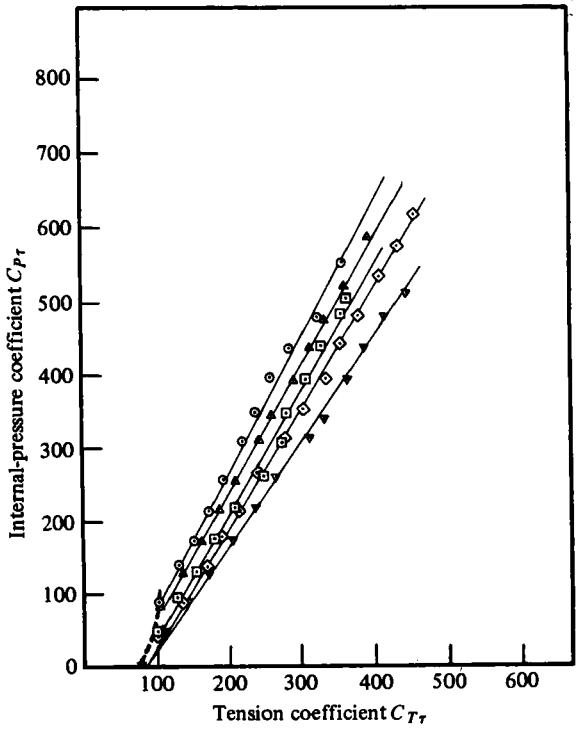

FIGURE 9. Measured tension as a function of inflation pressure for roughness 2. Symbols as in figure 8.

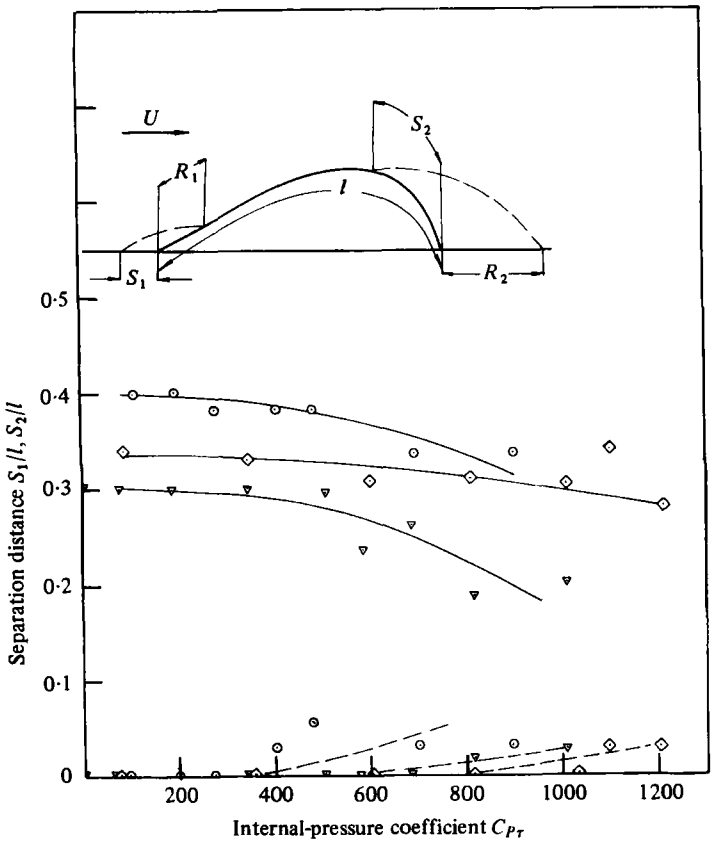

FIGURE 10. Separation distances at leading and trailing edge. Roughness 1. ▽, $(l-c)/c$ = 0·090; ◇, 0·154; ○, 0·266; ——, trailing-edge S_2/l; - - -, leading-edge S_1/l.

This is large but not excessively so for there exist full-scale stadia and greenhouses with widths not much smaller than this value.

An estimate of the solid and wake blockage of each model was obtained by considering an equivalent two-dimensional aerofoil in a *uniform* flow placed in a tunnel of twice the height. The solid-blockage correction to dynamic pressure ranged from 0·3 to 0·6 % depending on the height of the model, and Glauert's correction for wake blockage varied from 1·2 to 1·9 % (Pankhurst & Holder 1952). The combined corrections were applied to all the measurements of $C_{T\tau}$, $C_{P\tau}$ and $C_{p\tau}$, even though these coefficients are based on the skin friction velocity U_τ and the flow was not uniform.

4. Experimental results and comparison with theory

Measurements were made on five model buildings with $(l-c)/c$ ranging from 0·090 to 0·266, which corresponded to h/c from 0·186 to 0·328 for a range of gauge pressures from 0 to 44 Pa. The measurements of tension on five models for the two roughnesses are shown in figures 8 and 9. The results lie on nearly straight lines and are mutually consistent. They show, as would be expected, that the tension increases as the height of the building is reduced. The heavy dotted line on these figures indicates

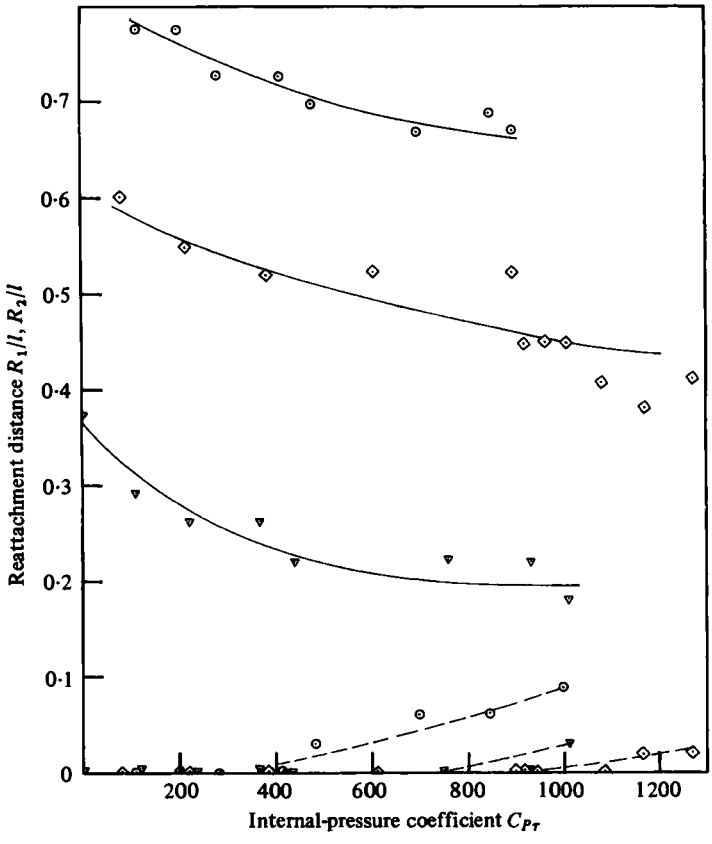

FIGURE 11. Reattachment distances at leading and trailing edges. Roughness 1. ▽, $(l-c)/c$ = 0·090; ◇, 0·154; ○, 0·266; ——, trailing-edge R_2/l; – – –, leading-edge R_1/l.

the onset of instability as the internal pressure was reduced. This occurred soonest on the highest buildings and started as an irregular oscillation followed by partial collapse at the leading edge.

Some separation and reattachment distances of the boundary layer at the leading and trailing edges are given in figures 10–13. They are shown to vary with the internal-pressure coefficient as well as with the height of the model. The size of the separation bubble is in general a great deal bigger at the trailing edge than it is at the leading edge. It is also bigger for the boundary layer with smaller roughness (roughness 1). Rather interestingly, the reattachment distances at the trailing edge decreased with increasing inflation pressure, which can be attributed to the change of shape towards a circular profile as the pressure is increased (see figure 14).

Further measurements were made near the end plates for roughness 2 as a check on the two-dimensionality of the results. The separation and reattachment distances were affected by the boundary-layer development over the plates and also by the leakage of air from inside the model itself. The distances were therefore sometimes larger and sometimes smaller than the centre-line values shown in figures 12 and 13. However, it was found that these variations were less than twice the experimental uncertainty of the presented results, which was estimated to be 0·05 of the membrane length l.

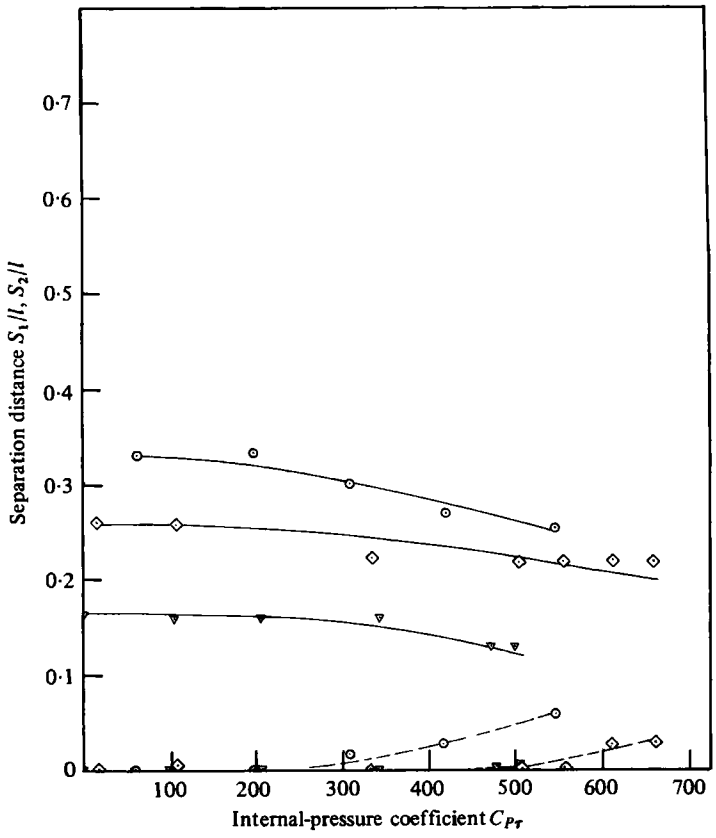

FIGURE 12. Separation distances at leading and trailing edges. Roughness 2. Symbols as in figure 10.

It is interesting to compare the tension measurements for the lowest building ($h/c = 0{\cdot}186$) with the thin-aerofoil theory of Newman & Tse (1980) (the line $a/c \to \infty$ in figure 6). To do this, the boundary-layer velocity corresponding to the top of the building was chosen to non-dimensionalize the results. The comparison is given in figure 15, and shows that the theory underestimates the tension by 6 % or less for roughness 1 and by 20 % or less for roughness 2.

The results for the lowest model were also used to choose the best matching procedure for the theory which is presented in this paper. The separation and reattachment bubbles are then smallest and this source of error is thereby minimized. The extreme pressures at the leading edge and at the top of the model are compared with the theory for both boundary layers in table 2. It is seen that matching method 2 is best, followed by method 1. Method 2 was therefore used in the subsequent comparisons.

The values of a/c from matching method 2 for the two roughnesses are given in table 3 for various lengths h/c and membrane lengths $(l-c)/c$. For the lowest model the values are 1·24 and 0·59. In figure 15 the results are compared with the theory shown in figure 6 for various a/c, and agreement is much better for roughness 1 than for roughness 2. However, this is not particularly significant because $(l-c)/c$ is too large.

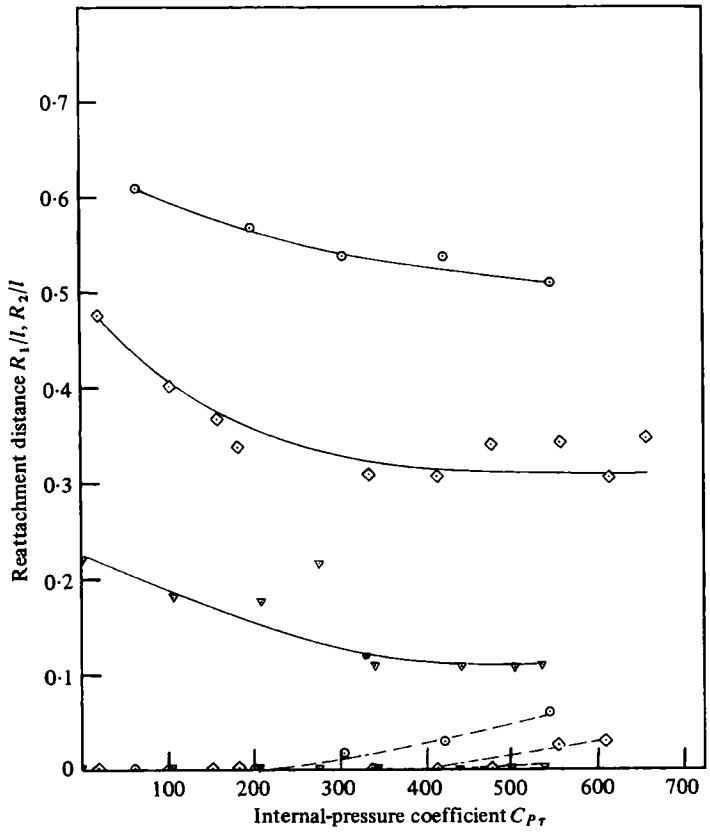

FIGURE 13. Reattachment distances at leading and trailing edges. Roughness 2. Symbols as in figure 11.

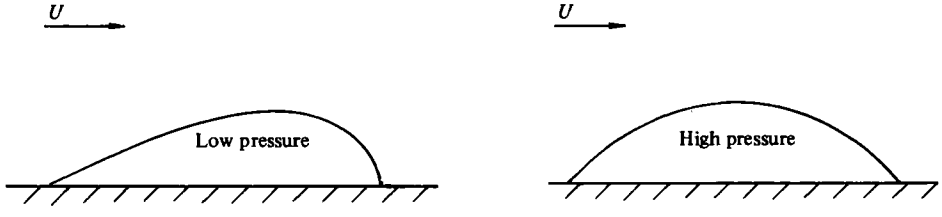

FIGURE 14. Sketches indicating the change of membrane shape with internal pressure.

It is worth noting that the theory of Hess & Smith predicts the value of $(l-c)/c$ from chosen values of C_T and C_P. To find C_T for a given combination of $(l-c)/c$ and C_P, which is the experimental situation, therefore requires a series of trial computations to obtain the desired value of $(l-c)/c$. This has been done for the six cases shown in figure 16, where the distributions are compared with the experimental results. The abscissa for these figures has been chosen as the non-dimensional arc distance s/l, since it was easier to identify the position of the pressure probe in relation to the membrane itself. All the experimental results show a constant-pressure region at the front and back corresponding to the separation bubbles there. This feature is, of

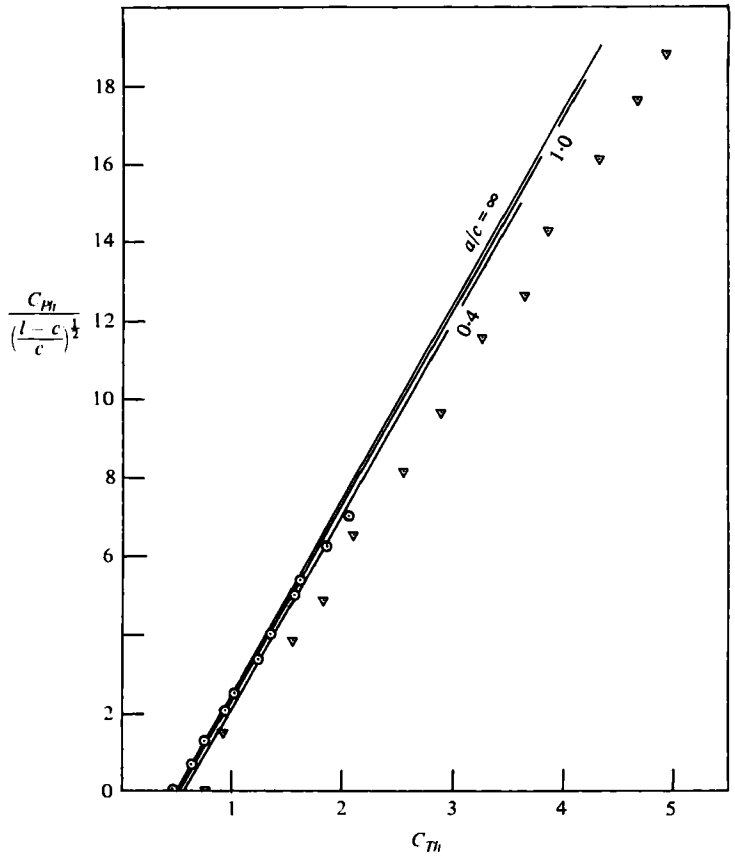

FIGURE 15. Tension coefficient as a function of combined pressure coefficient for $(l-c)/c = 0{\cdot}09$. $h/c = 0{\cdot}186$. Comparison between experiment, thin-aerofoil theory and the present theory, ⊙, $n^{-1} = 0{\cdot}13$, $a/c = 1{\cdot}24$; ▽, 0·24, 0·59; ——, thin-aerofoil theory.

	$C_{pT\max}$	$C_{pT\min}$	C_{T_T}
Experiment	35	−109	225
Theory using matching method			
1	48·2	−115	220
2	44·5	−110	201
3	50	−116	218

TABLE 2. Comparison of three methods for matching a flow of uniform vorticity to a boundary layer as represented by a power law; $(l-c)/c = 0{\cdot}090$, $C_{P_T} = 209$, $n^{-1} = 0{\cdot}24$

$\frac{l-c}{c}$	$\frac{h}{c}$	a/c Roughness 1 ($n^{-1} = 0{\cdot}13$)	a/c Roughness 2 ($n^{-1} = 0{\cdot}24$)
0·266	0·328	2·20	1·04
0·231	0·304	2·03	0·96
0·164	0·254	1·70	0·80
0·154	0·246	1·65	0·78
0·090	0·186	1·24	0·59

TABLE 3. Values of a/c using matching method 2

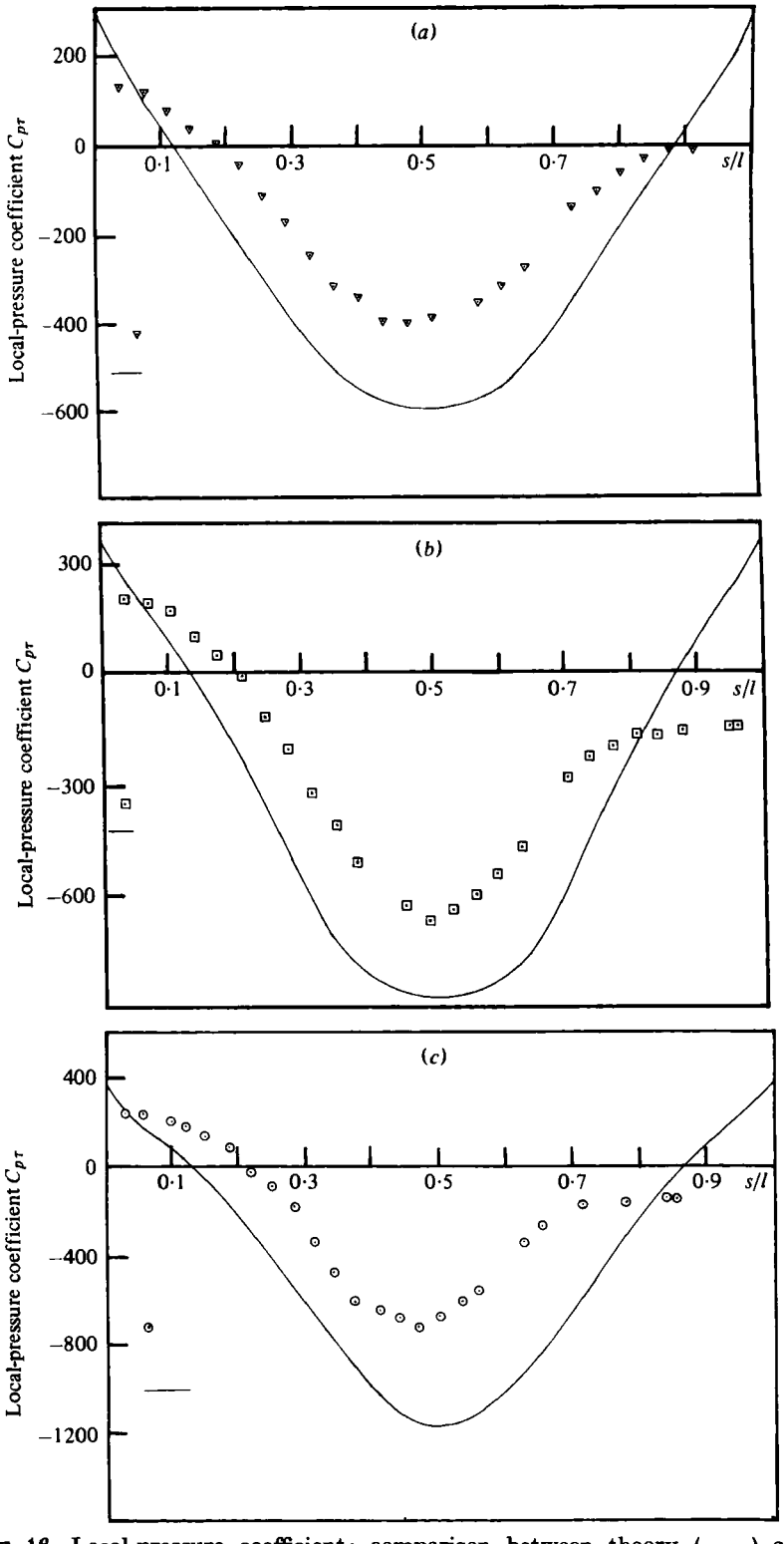

FIGURE 16. Local-pressure coefficient: comparison between theory (——) and experiment (▽, ⊡, ⊙). Roughness 1: (*a*) $(l-c)/c$ = 0·090, C_{P_T} = 646; (*b*) 0·164, 974; (*c*) 0·266, 666. Roughness 2: (*d*) 0·090, 209; (*e*) 0·164, 181; (*f*) 0·266, 221.

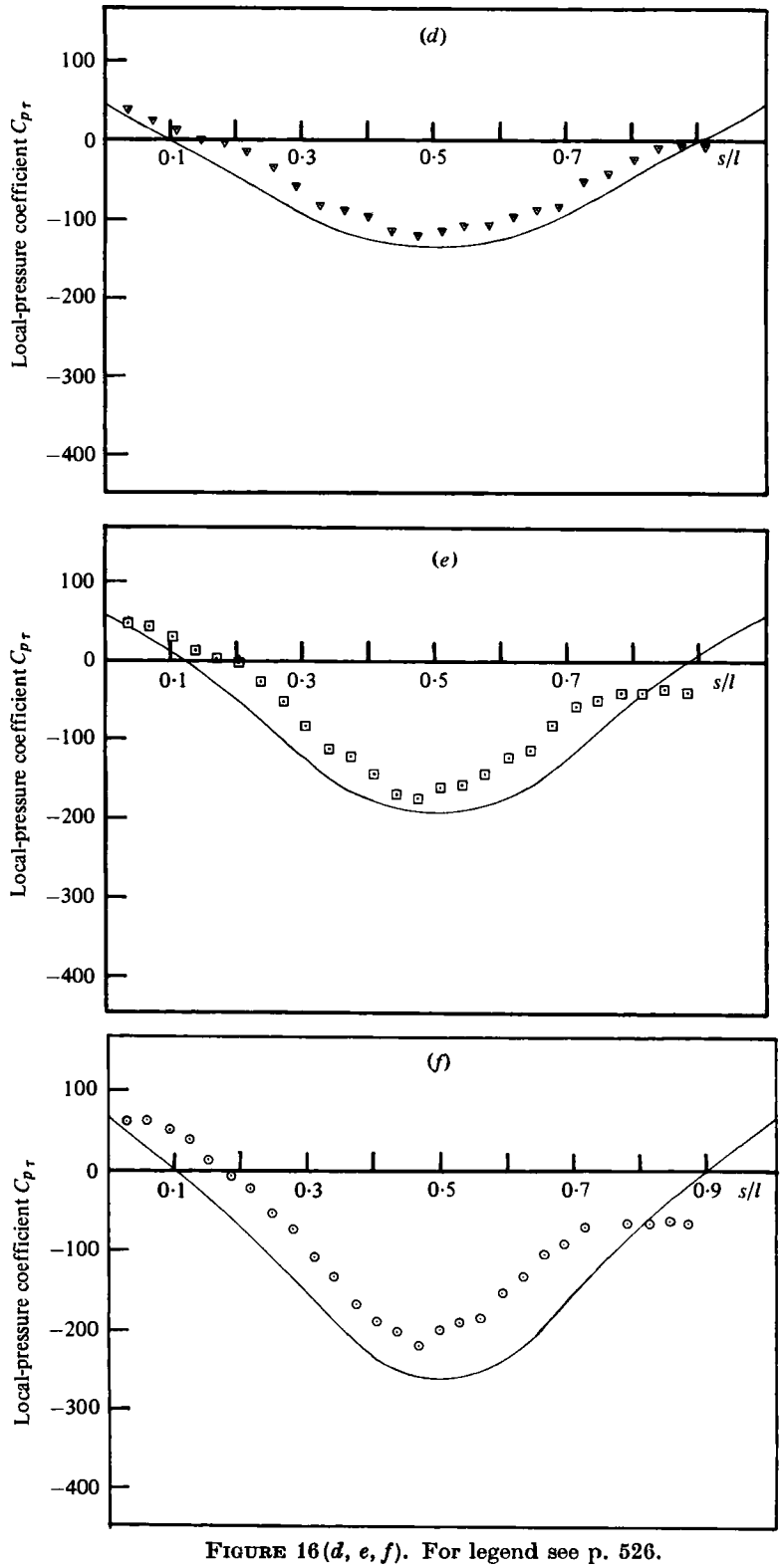

FIGURE 16 (*d*, *e*, *f*). For legend see p. 526.

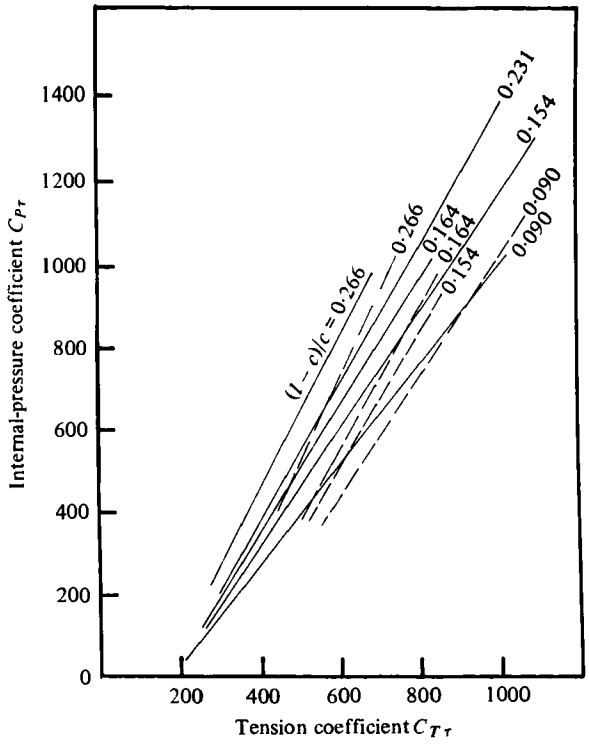

FIGURE 17. Tension as a function of internal pressure. Comparison between theory (– – –) and experiment (——). Roughness 1.

course, missing from the theoretical curves. Over most of the membrane the predicted pressures are lower than the data. The agreement between theory and experiment is better for the rougher surface, presumably because the separation bubbles are smaller in this case.

The predictions for the membrane tension are shown in figures 17 and 18, where they are compared with the experimental results. In general the agreement is fair and, rather surprisingly, the discrepancy is not all of the same sign.

Further cases were computed using matching method 1. The predicted tension coefficient C_{T_τ} was very similar but slightly closer to the experimental results than the present predictions using matching method 2. The improvement was usually less than 1 % of C_{T_τ}. However, the pressure distribution was not so well predicted in general. For example at the maximum height of the model the discrepancy between prediction and experiment was increased by typically 5 %.

It should be noted that the Reynolds number $U_\tau c/\nu$ of the present model tests is between 4000 and 6000, and is very much lower than that of a full-scale building. The terrain may usually be classified as 'fully rough' in the aerodynamic sense and thus the boundary layer approaching the building is not sensitive to changes of Reynolds number. However, the flow over the building itself and in particular the separation and reattachment distances may be sensitive to scale effect. With increasing Reynolds number these distances tend to become smaller. Thus the discrepancies between the present theory and experiment will be reduced for full-scale buildings.

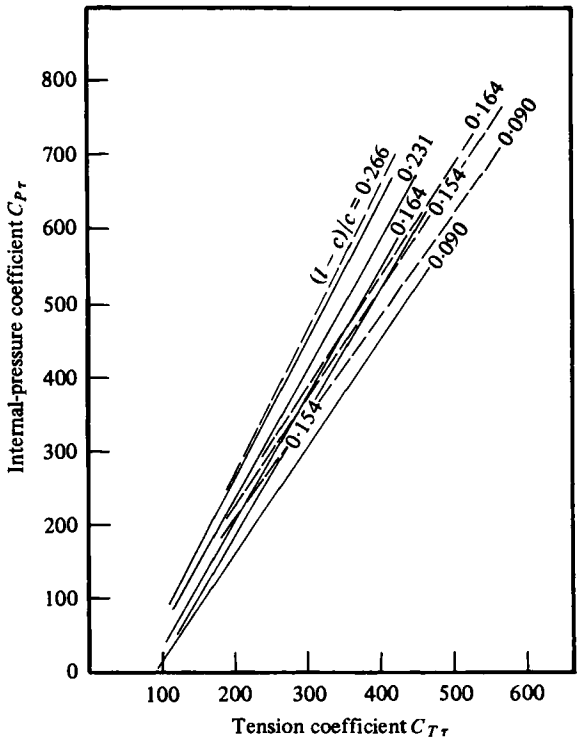

FIGURE 18. Tension as a function of internal pressure. Comparison between theory (– – –) and experiment (——). Roughness 2.

	Terrain				
	Near open sea	Flat open country	Sparsely wooded country	Wooded country	Urban centre
n^{-1}	0·13	0·16	0·24	0·28	0·40
U_{10}/U_τ	15·9	12·1	6·15	4·65	1·98

TABLE 4. Natural-wind data and the ratio of U at 10 m to the skin-friction velocity U_τ (based on Devenport (1963))

Estimates of membrane tension, which may be useful for building design, can therefore be obtained by a judicious use of both the theoretical and experimental information presented in this paper. The procedure for estimating the tension in a long full-scale building subjected to a cross wind might be as follows. The exponent n^{-1} of the wind boundary layer depends on the terrain, and values may be obtained from table 4 or from Davenport (1963). The wind velocity U_{10} at a standard height of, say, 10 m would be known. The value of U_{10}/U_τ for the chosen n^{-1} may be obtained from table 4. Thus U_τ is known and the internal-pressure coefficient $C_{P\tau}$ may be calculated. Knowing $(l-c)/c$ figures 17 and 18 give both theoretical and experimental estimates of $C_{T\tau}$, and hence the membrane tension for the building.

REFERENCES

BEGER, G. & MACHER, E. 1967 Results of wind-tunnel tests on some pneumatic structures. In *Proc. 1st Int. Colloq. on Pneumatic Structures, Stuttgart*, pp. 142–146.

BIRD, W. W. & KAMRASS, M. 1956 Design for spherical air-supported radomes. *Cornell Aero. Lab. Rep.*. UB-909-D-2.

CAMPBELL, S. & STANDEN, N. M. 1969 Progress report II on simulation of Earth's boundary layer by artificially thickened wind-tunnel boundary layers. *NRC NAE Rep.* LTR-LA-37.

COLES, D. 1956 The law of the wake in a turbulent boundary layer. *J. Fluid Mech.* **1**, 191–226.

COOK, N. J. 1973 On simulating the lower third of the urban adiabatic boundary layer in a wind tunnel. *Atmos. Environ.* **7**, 691–705.

COOK, N. J. 1977 Determination of the model scale factor in wind-tunnel simulations of the adiabatic atmospheric boundary layer. *J. Ind. Aerodyn.* **2**, 311–321.

DAVENPORT, A. G. 1963 The relationship of wind structure to wind loading. In *Proc. Conf. on Wind Effects on Buildings and Structures, N.P.L., Teddington*, pp. 54–65.

GARTSHORE, I. S. & DE CROOS, K. A. 1977 Roughness element geometry required for wind-tunnel simulations of the atmospheric wind. *Trans. A.S.M.E.* I, *J. Fluids Engng* **99**, 480–485.

HERZOG, T. 1976 *Pneumatic Structures*. Oxford University Press.

HESS, J. L. & SMITH, A. M. O. 1967 Calculation of potential flow about arbitrary bodies. *Prog. Aero. Sci.* **8**, 1–138.

IRWIN, H. P. A. H. 1972 The longitudinal cooling correction for wires inclined to the prongs and some turbulence measurements in fully developed pipe flow. *Mech. Engng Res. Lab., McGill University, Tech. Note* no. 72–1.

KAMRASS, M. 1954 Wind-tunnel tests on a $\frac{1}{24}$th scale model air-supported radome and tower. *Cornell Aero. Lab. Rep.* UB-909-D-1.

MILNE-THOMSON, L. M. 1968 *Theoretical Hydrodynamics*, 5th edn, p. 177. Macmillan.

NEWMAN, B. G. & TSE, M.-C. 1980 Flow past a thin, inflated, lenticular aerofoil. *J. Fluid Mech.* **100**, 673–689.

NIEMANN, H.-J. 1972 Wind-tunnel experiments on aeroelastic models of air-supported structures. In *Proc. Int. Symp. on Pneumatic Structures, Delft.* Paper No. 5–11.

OTTO, F. & TROSTEL, R. 1973 *Tensile Structures*. M.I.T. Press.

PANKHURST, R. C. & HOLDER, D. W. 1952 *Wind-Tunnel Technique*. Pitman.

PLATE, E. J. 1971 Aerodynamic characteristics of atmospheric boundary layers. *U.S. Atomic Energy Comm.* TID-25465.

SMITH, D. W. & WALKER, J. H. 1958 Skin-friction measurements in incompressible flow. *N.A.C.A. Tech. Note* no. 4231.

STANDEN, N. M. 1972 A spire array for generating thick turbulent shear layers for natural wind simulation in wind-tunnels. *NRC NAE Rep.* LTR-LA-94.

VOGEL, W. M. 1968 General description and calibration of the McGill 30 inch diameter blower wind-tunnel. *Mech. Engng Res. Lab., McGill University, Tech. Note*, no. 68–1.